PNAS
www.pnas.org

Supplementary Information for
Interleukin-2 superkines by computational design

Junming Ren*, Alexander E. Chu*, Kevin M. Jude*, Lora Picton, Aris J. Kare, Leon Su, Alejandra Montano Romero, Po-Ssu Huang#, K. Christopher Garcia#

Po-Ssu Huang#, K. Christopher Garcia#
Email: kcgarcia@stanford.edu, possu@stanford.edu

This PDF file includes:

Figures S1 to S12
Tables S1 and S2

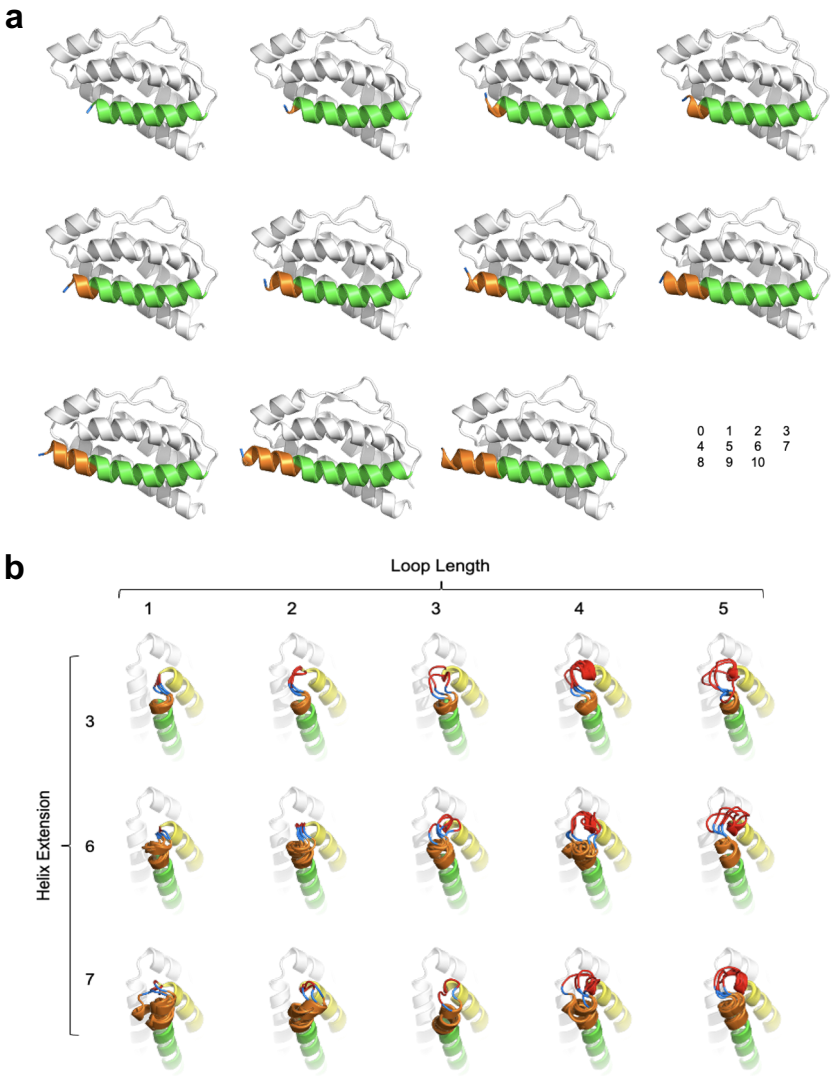

Fig. S1. Topology Redesign.

(A) Example trajectories for each of several sampled helix D extension lengths. Helix D is highlighted in green, the capping residue is in blue, and the modeled extensions are in orange. Corresponding extension lengths as indicated in bottom right corner.
(B) Example trajectories from joint modeling and grid search of helix C extensions with BC-loop lengths

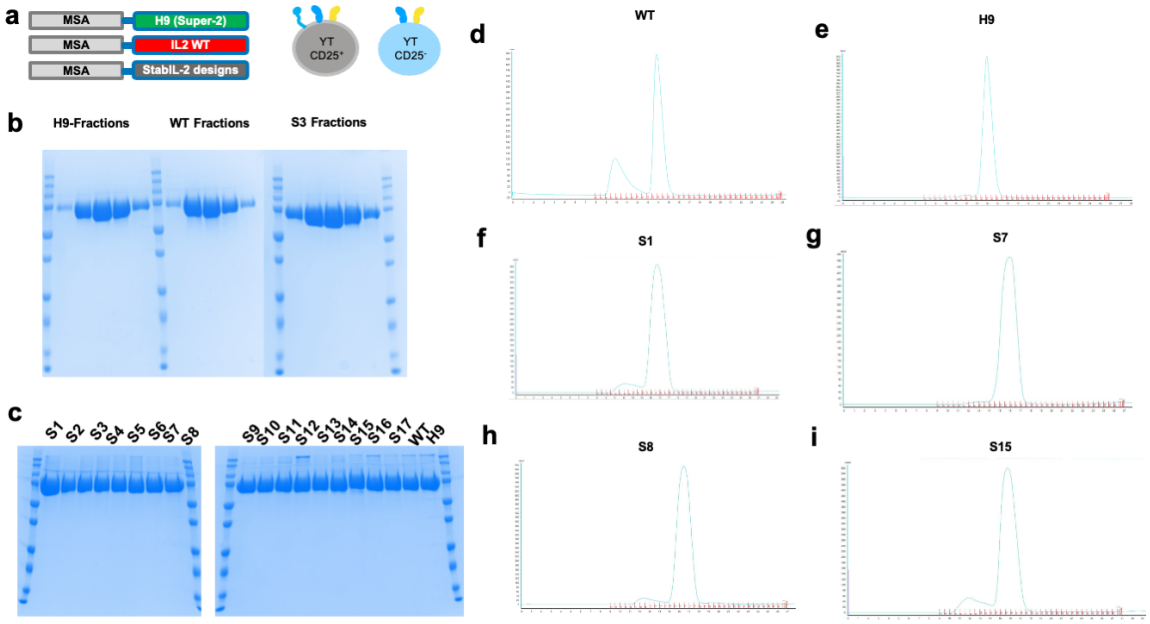

Fig. S2. StabIL-2 expression in expi293 cells.

(A) Construct used for MSA fusions of stabIL-2 variants and illustration of $CD25^{+}$ and $CD25^{-}$ YT cells.
(B-C) Coomassie blue staining of purified stabIL-2 variants.
(D-I) Representative FPLC (gel filtration) traces for (D) WT, (E) super-2 H9, (F) S1, (G) S7, (H) S8, and (I) S15.

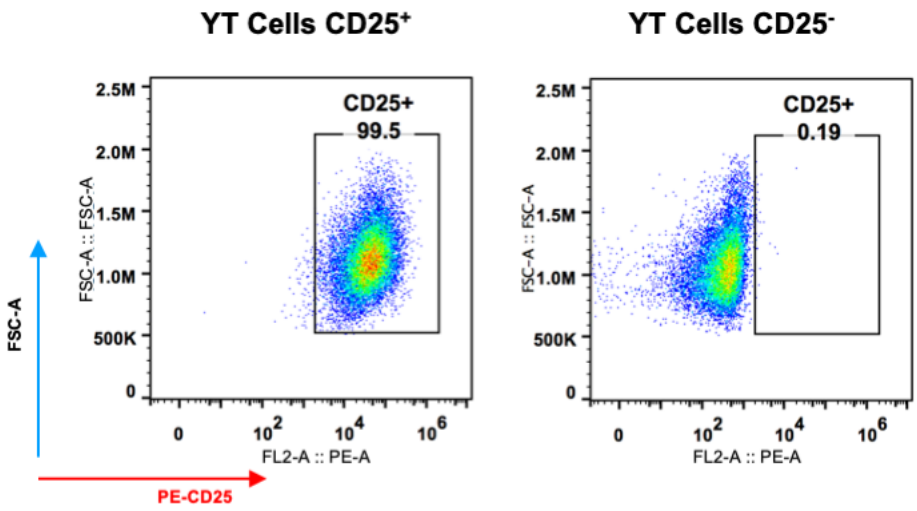

Fig. S3. Flow cytometry of YT cells on CD25 expression.

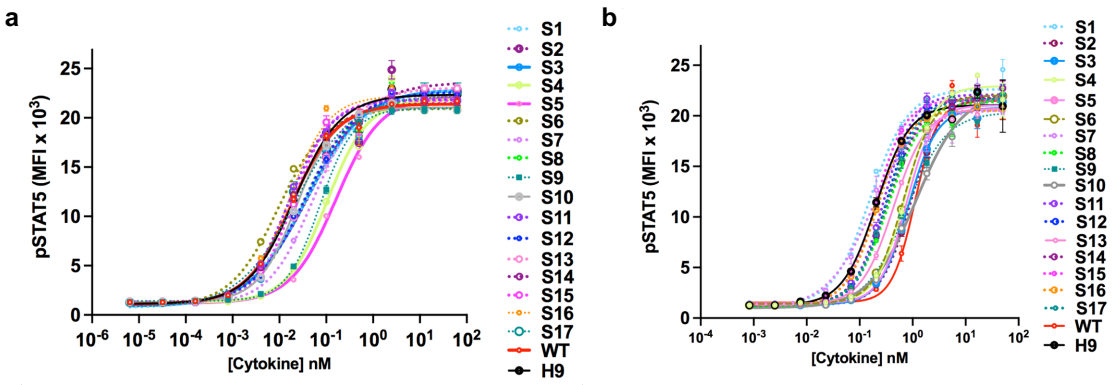

Fig. S4. Stat5 phosphorylation in CD25+ (a) and CD25- (b) YT cells.

Data are shown as mean ± standard deviation of triplicate wells and are representative of two independent experiments.

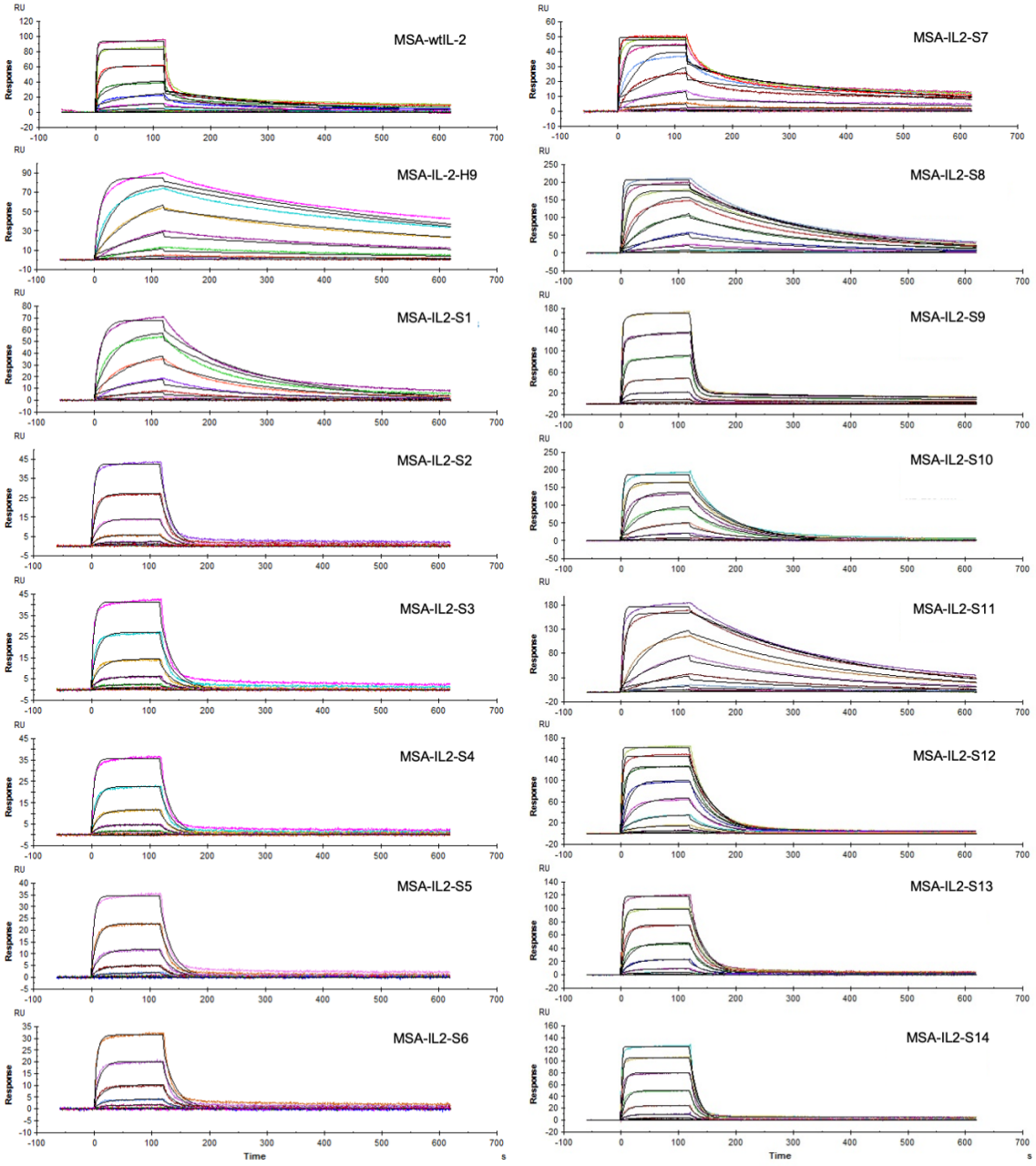
MSA-wtIL-2
MSA-IL-2-H9
MSA-IL2-S1
MSA-IL2-S2
MSA-IL2-S3
MSA-IL2-S4
MSA-IL2-S5
MSA-IL2-S6
MSA-IL2-S7
MSA-IL2-S8
MSA-IL2-S9
MSA-IL2-S10
MSA-IL2-S11
MSA-IL2-S12
MSA-IL2-S13
MSA-IL2-S14
RU
Response
Time
s

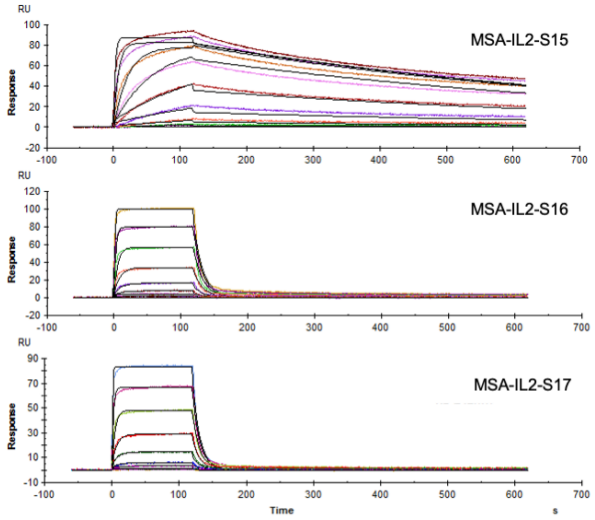

Fig. S5. SPR kinetic traces for all stablL-2 designs.

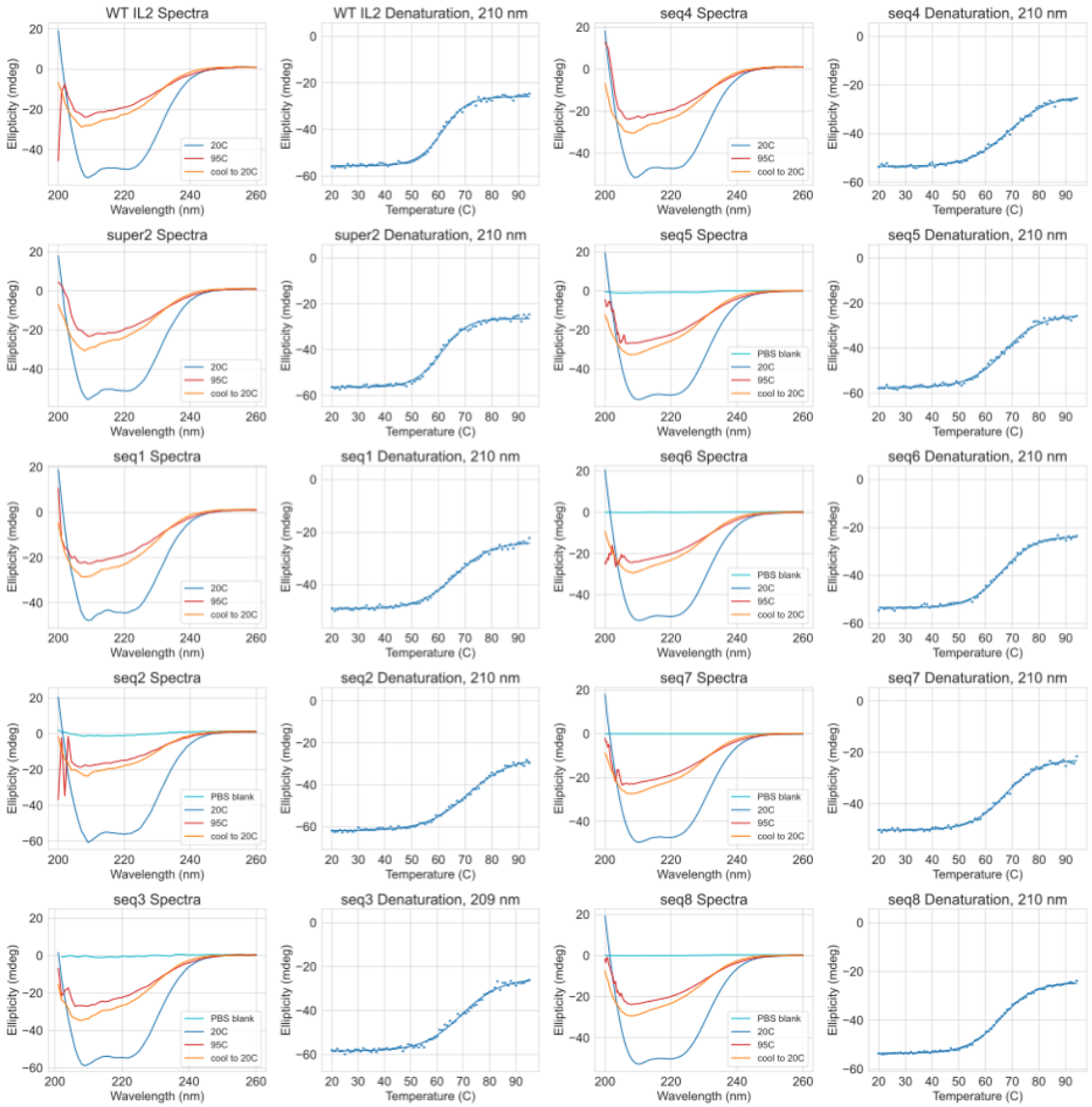

Fig. S6. Secondary structure and thermal stability of stabIL-2 proteins tagged with MSA. Spectra plot legends correspond to the temperature that the spectrum was measured at; “cool to 20C” indicates a spectrum measured after the sample was cooled to 20°C again after the denaturation experiment. Where indicated, “PBS blank” indicates a spectrum measured at 20°C in phosphate buffer before the denaturation experiment.

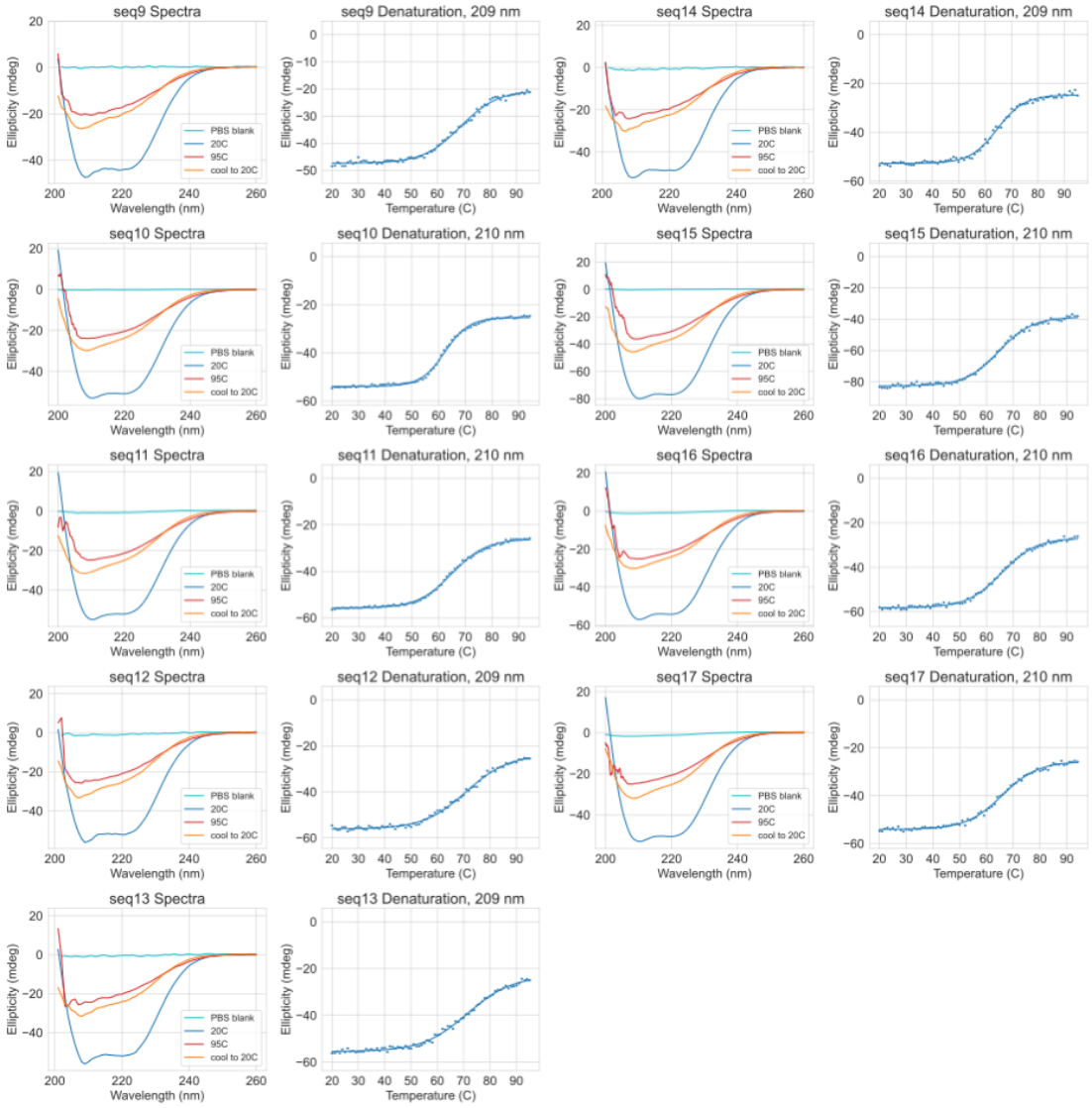

Fig. S6 (continued). Secondary structure and thermal stability of stabIL-2 proteins tagged with MSA.

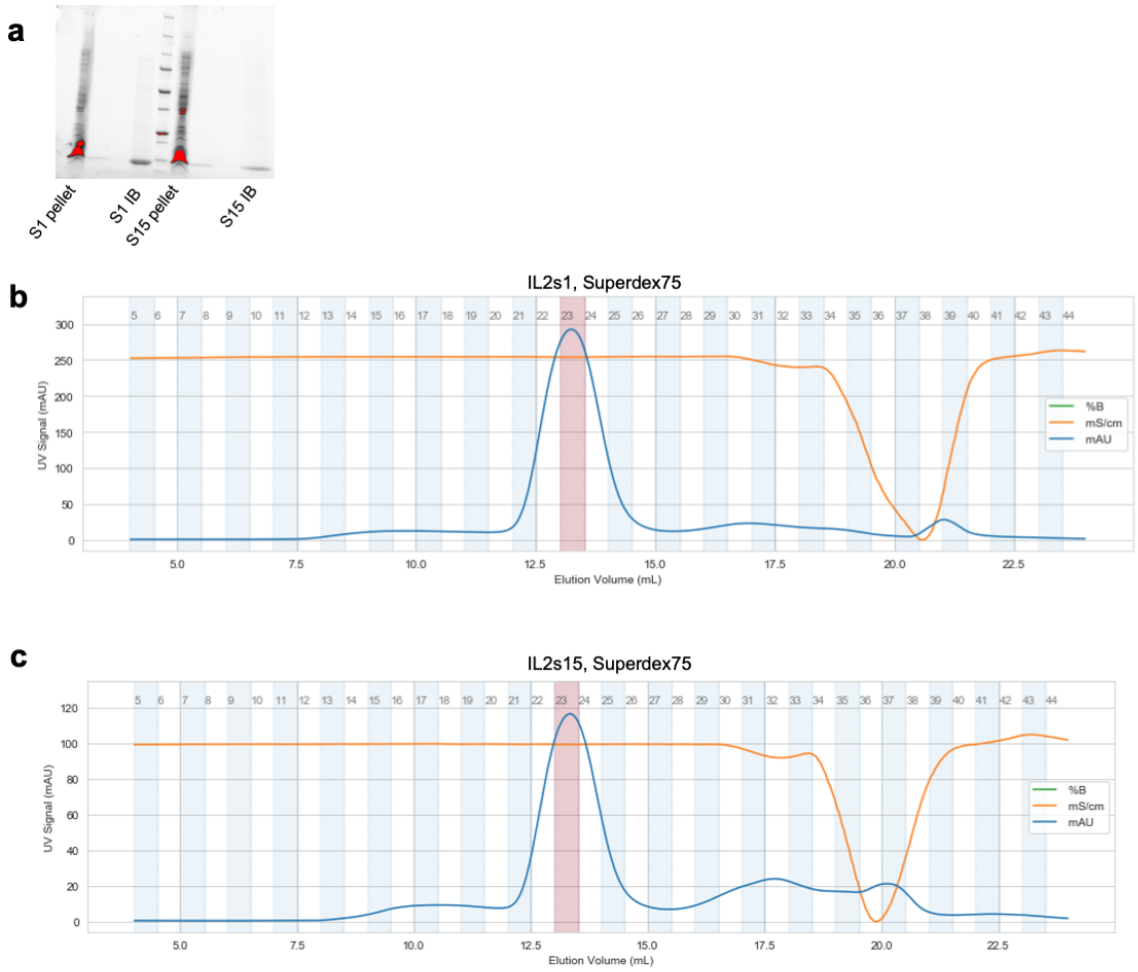

Fig. S7. Expression of tagless stabIL-2 variants in E. coli and purification.

(A) Gel of solubilized inclusion bodies.
(B) FPLC gel filtration (superdex75) trace for S1; fraction marked in red was used for CD.
(C) FPLC gel filtration (superdex75) trace for S15; fraction marked in red was used for CD.

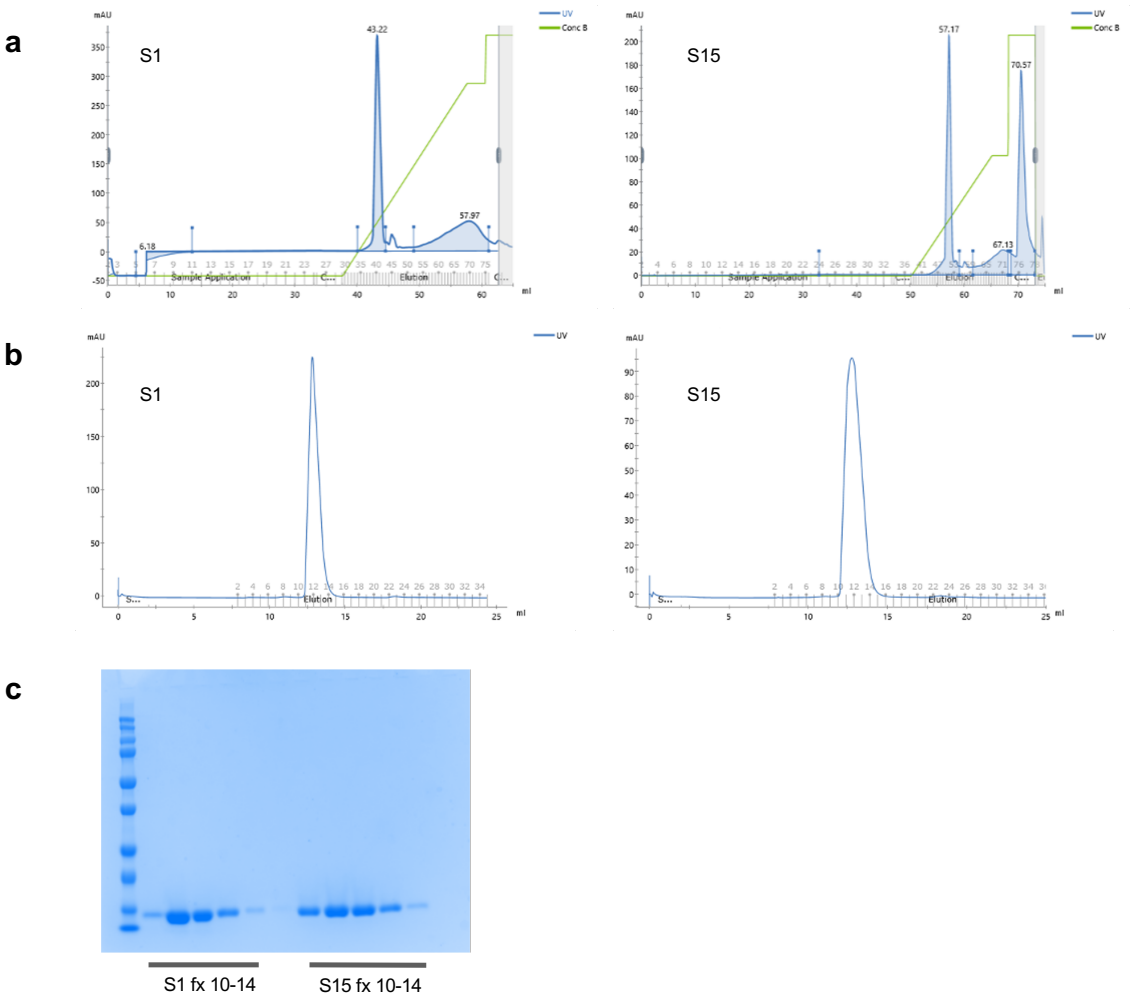

Fig. S8. Representative purifications of S1 and S15 for crystallization.

(A) MonoQ chromatograms for refolded S1 (left) and S15 (right). The first peak from each column was pooled and concentrated for further purification
(B) Gel Filtration (S75) chromatograms for S1 (left) and S15 (right)
(C) Coomassie-stained SDS PAGE gel of S75 fractions used for crystallization

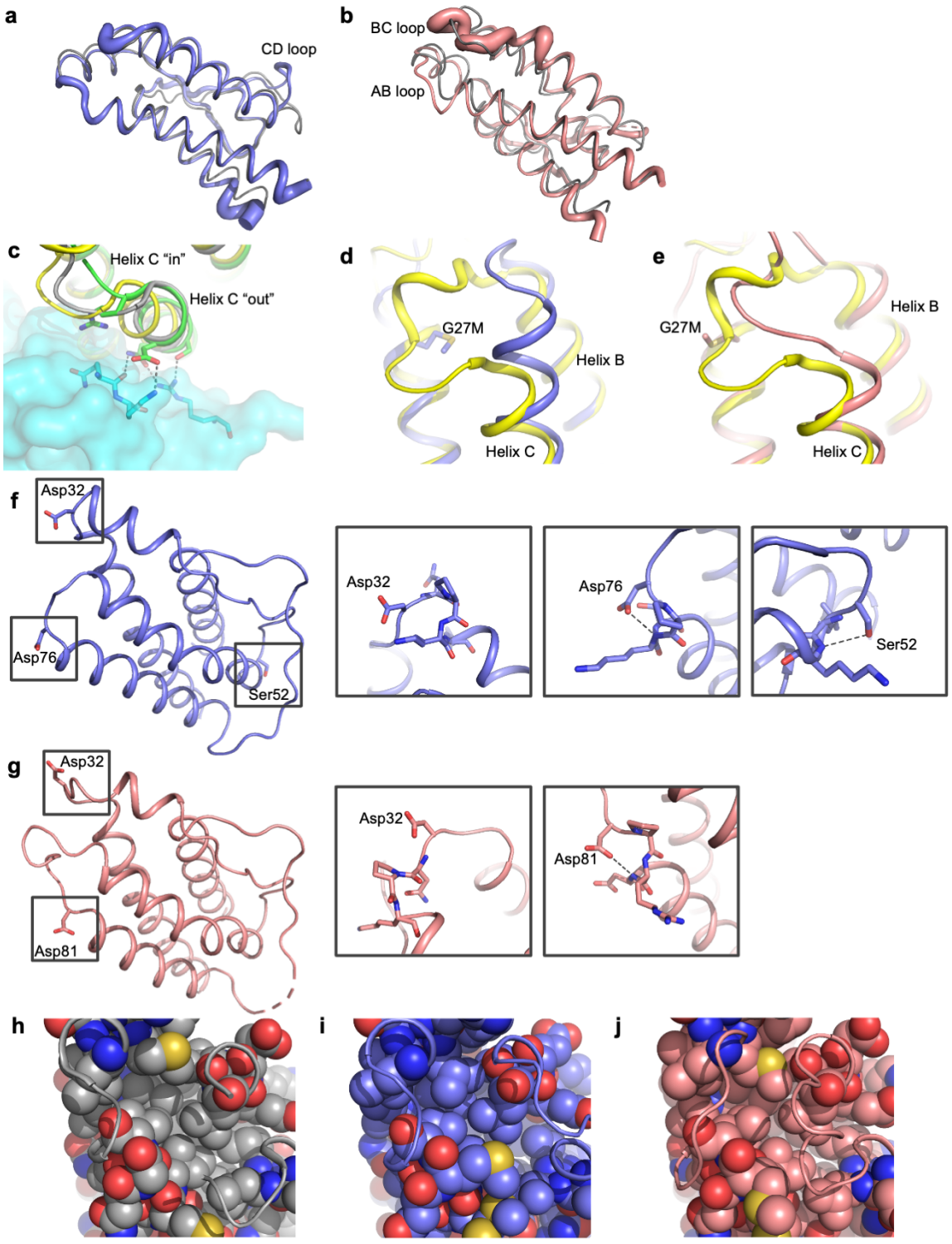

Fig. S9. IL-2Rβ binding conformation is stabilized in S1 and S15

(A, B) Crystal structures of S1 (slate) and S15 (salmon) superimposed on their respective design models (gray). The crystal structures are shown in putty representation, with the width of the backbone cartoon proportional to the B-factor at the Ca atom for each residue.

(C) Structural alignment of apo-in (3INK, yellow), apo-out (1M47, gray), and receptor-bound (2B5I, green) IL-2. Hydrogen bond interactions between IL-2 helix C and IL-2Rβ (cyan) are shown as dashed lines.
(D, E) Alignment of S1 (slate) and S15 (salmon) crystal structures with apo-in IL-2. The introduced Met sidechain at position 27 is shown in stick representation.
(F, G) Designed helical capping residues in S1 (slate) and S15 (salmon). Successful capping hydrogen bonds observed in the crystal structures are shown as dashed lines.
(H-J) Atomic packing of wt IL-2 (1M47, gray), S1 (slate), and S15 (salmon) shown as van der Waals spheres. Portions of the AB and BC loops are shown as cartoons for clarity.

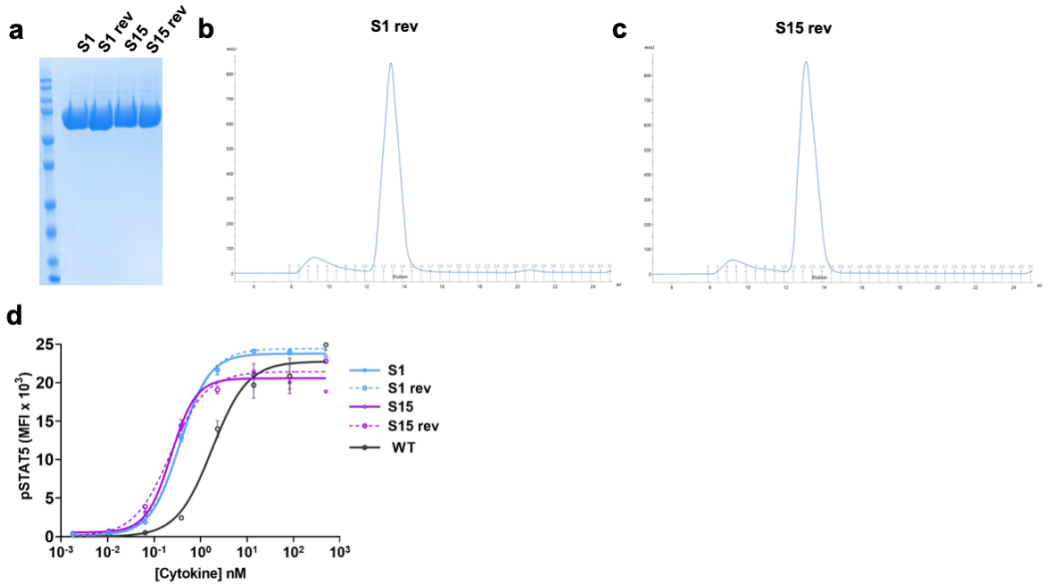

e

								Mutation number	EC50 in CD25- YT (nM)
Residue no.	**27**	**28**	**32**	**69**	**72**	**81**	**115**		
WT IL-2	G	I	K	V	L	R	V	0	1.18
S15	M	L	D	A	Q	D	I	7	0.108
S15 rev	M	I	D	V	Q	D	V	4	0.11

										Mutation number	EC50 in CD25- YT (nM)
Residue no.	**27**	**28**	**32**	**39**	**52**	**69**	**72**	**loop**	**115**		
WT IL-2	G	I	K	M	E	V	L	AQSKNFHL	V	0	1.18
S1	M	L	D	L	S	A	A	GDDPKTI	I	7	0.108
S1 rev	M	L	D	L	S	V	A	GDDPKTI	V	4	0.11

Fig. S10. Partial reversions of S1 and S15 to wild type maintain the same activity.

(A) Coomassie blue staining of purified S1 rev and S15 rev compared with original S1 and S15.
(B-C) FPLC gel filtration traces for S1 rev (B) and S15 rev (C).
(D) pStat5 activation assay of S1 rev and S15 rev, compared with WT and original S1, S15.
(E) Reverting mutations and EC50 values calculated from (D). Data are shown as mean ± standard deviation of triplicate wells and are representative of two independent experiments.

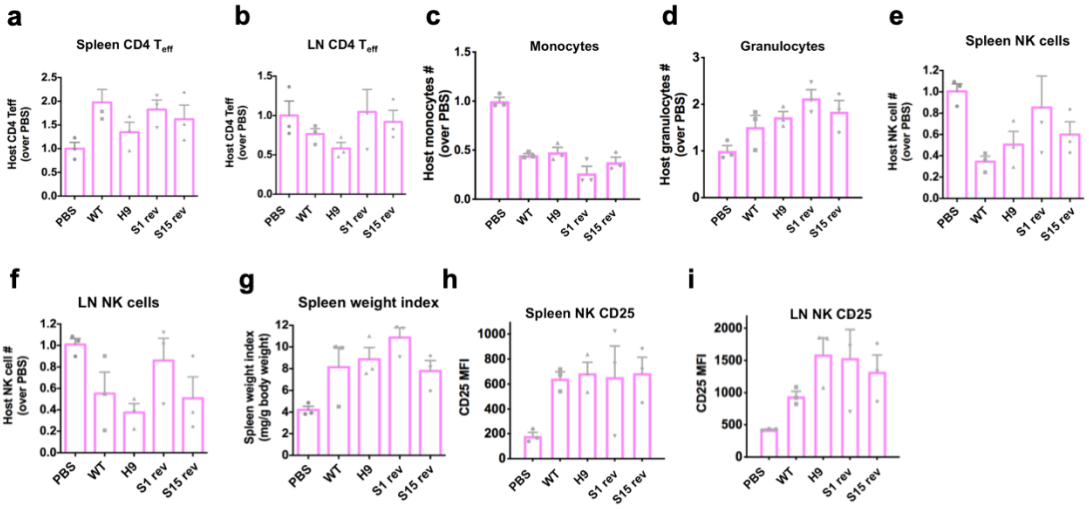

Fig. S11. In vivo activity of stabIL-2 designs.

(A-F) Quantification of stabIL-2's administration on C57BL/6 mice
(A, B) CD4 effector T cells (Teff, $CD44^{+}CD62L^{-}$), (C) monocytes, (D) granulocytes, (E) natural killer (NK) cell ($CD3^{-}NK1.1^{+}NKp46^{+}$) in spleen and (F) lymph nodes.
(G) Spleen weight normalized to total body weight on day of sacrifice.
(H, I) Quantification of CD25 expression on NK cells in (H) spleen and (I) lymph nodes of cytokines treated mice. Bar graphs show mean ± standard deviation. Data are representative of three independent experiments.

Example flags used for RosettaRemodel

```
-in:file:s 1m47_clean.pdb
-remodel:blueprint
design0.bp
-jd2:no_output
-overwrite
-soft_rep_design
-num_trajectory 1
-save_top 1
-remodel:use_pose_relax
-remodel:dr_cycles 3
-ex1
-ex2
-no_optH false
-linmem_ig 10
```

Example logo plot (after 2 iterations)

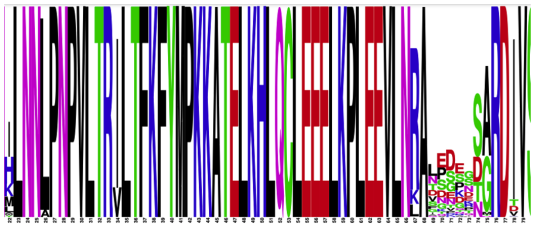

Example blueprints for specifying design

Initial

```
…
21 N .
22 G . ALLAAxc
23 I . ALLAAxc
24 N .
25 N .
26 Y . ALLAAxc
27 K . ALLAAxc
28 N .
29 P .
30 K . ALLAAxc
31 L .
32 T .
33 R .
34 M . ALLAAxc
35 L .
…
46 T .
47 E . PIKAA DNST
48 L .
…
63 E .
64 V . ALLAAxc
65 L .
66 N .
67 L . ALLAAxc
68 A .
69 Q L ALLAAxc
70 N L ALLAAxc
71 F L ALLAAxc
72 H L ALLAAxc
73 L L ALLAAxc
74 R L PIKAA DNST
75 P L ALLAAxc
76 R .
77 D .
78 L . ALLAAxc
79 I . ALLAAxc
80 S .
…
84 V .
85 I . ALLAAxc
86 V .
…
103 I .
104 V . ALLAAxc
105 E .
…
```

After 2 iterations

```
…
21 N .
22 H . PIKAA IHKMLA
23 L . PIKAA L
24 N .
25 N .
26 L . PIKAA LA
27 P . PIKAA P
28 N .
29 P .
30 V . PIKAA V
31 L .
32 T .
33 R .
34 I . PIKAA IV
35 L .
…
46 T .
47 D . PIKAA DS
48 L .
…
63 E .
64 V . PIKAA V
65 L .
66 N .
67 R . PIKAA RKL
68 A .
69 D L PIKAA LNTDVSFG
70 N L PIKAA EPSDNGKT
71 Q L PIKAA DSGENTVP
72 P L PIKAA ESPKDGQT
73 G L PIKAA GSNDEKRPT
74 S L PIKAA DNST
75 A L PIKAA AGM
76 R .
77 D .
78 I . PIKAA ITDV
79 V . PIKAA V
80 S .
…
84 V .
85 I . PIKAA IV
86 V .
…
103 I .
104 I . PIKAA IL
105 E .
…
```

Fig. S12. Rosetta design scripts.

Supplementary Table S1. Rates and equilibrium constants for binding to IL-2Rβ determined by SPR

Protein	k_a ($M^{-1}s^{-1}$)	k_d (s^{-1})	K_d kinetic (nM)	K_d steady state (nM)
wt MSA-hIL2	1.33 e 5	4 e -3	30	374
MSA-hIL2 H9	7.6 e 5	1.5 e -3	2.1	16
MSA-S1	2.7 e 5	6.6 e -3	25	61
MSA-S2	1.67 e 5	5.5 e -2	330	411
MSA-S3	1.5 e 5	4.2 e -2	280	366
MSA-S4	1.47 e 5	5.0 e -2	340	389
MSA-S5	1.6 e 5	4.7 e -2	290	362
MSA-S6	1.5 e 5	4.6 e -2	320	398
MSA-S7	1.89 e 6	9.545 e -3	5.05	24.4
MSA-S8	7.7 e 5	4.4 e -3	5.9	14.2
MSA-S9	3.7 e 5	1.23 e -1	330	378
MSA-S10	1.5 e 5	1.5 e -2	110	137
MSA-S11	4.1 e 5	3.6 e -3	8.7	22.7
MSA-S12	4.6 e 5	2.3 e -2	51	67.6
MSA-S13	2.1 e 5	3.6 e -2	170	207
MSA-S14	4.2 e 5	7.2 e -2	170	196
MSA-S15	6.5 e 5	1.4 e -3	2.1	11.53
MSA-S16	3.2 e 5	7.1 e -2	220	290
MSA-S17	3.8 e 5	9.1 e -2	240	268

Table S2. Crystallographic data collection and refinement statistics.

	S1	**S15**
Wavelength	1.033167	0.97946
Resolution range	40.35 - 2.2 (2.279 - 2.2)	44.77 - 2.694 (2.904 - 2.694)
Ellipsoidal[a] resolution limit (Å) (direction)[b]	-	3.19 (**a***) 3.19 (**b***) 2.55 (**c***)
Space group	P 65 2 2	P 43 21 2
Unit cell (a,b,c (Å)) (α,β,γ (°))	46.588, 46.588, 234.255 90, 90, 120	66.372, 66.372, 298.302 90, 90, 90
Total reflections	139088 (6688)	377633 (17343)
Unique reflections	8217 (697)	13754 (688)
Multiplicity	16.9 (9.6)	27.4 (25.2)
Completeness (%)	95.97 (78.84)	70.56 (18.07)
Completeness (ellipsoidal)[c] (%)	-	93.4 (85.2)
Mean I/sigma(I)	5.78 (0.57)	16.30 (0.16)
Mean I/sigma(I) (ellipsoidal)[a]	-	20.71 (1.14)
R-meas	0.3092 (3.606)	0.105 (3.205)
R-pim	0.07409 (1.141)	0.020 (0.623)
CC1/2	0.998 (0.266)	1.00 (0.528)
Reflections used in refinement	8094 (626)	13749 (252)
Reflections used for R-free	809 (62)	822 (14)
R-work	0.2484 (0.3477)	0.2477 (0.3819)
R-free	0.2934 (0.4052)	0.2943 (0.3747)
Protein residues	126	496
ligand atoms	15	2
solvent atoms	36	14
RMS(bonds)	0.002	0.003
RMS(angles)	0.44	0.55
Ramachandran favored (%)	98.39	95.42
Ramachandran outliers (%)	0.00	0.00
Rotamer outliers (%)	0.00	5.97
Clashscore	2.38	6.84
Average B-factor	55.09	92.38
macromolecules	54.59	92.46
ligands	97.11	88.51
solvent	52.04	69.08

Statistics for the highest-resolution shell are shown in parentheses.

a These statistics are for data that were truncated by STARANISO to remove poorly measured reflections affected by anisotropy.
b The resolution limits for three directions in reciprocal space are indicated here. To accomplish this, STARANISO computed an ellipsoid postfitted by least squares to the cutoff surface, removing points where the fit was poor. Note that the cutoff surface is unlikely to be perfectly ellipsoidal, so this is only an estimate.
c The anisotropic completeness was obtained by least squares fitting an ellipsoid to the reciprocal lattice points at the cutoff surface defined by a local mean $I/\sigma I$ threshold of 1.0, rejecting outliers in the fit due to spurious deviations (including any cusp), and calculating the fraction of observed data lying inside the ellipsoid so defined. Note that the cutoff surface is unlikely to be perfectly ellipsoidal, so this is only an estimate.